*W. Brocks** and *G. Künecke**

On the Influence of Triaxiality of the Stress State on Ductile Tearing Resistance

REFERENCE Brocks, W. and Künecke, G., **On the influence of triaxiality of the stress on ductile tearing resistance,** *Defect Assessment in Components – Fundamentals and Applications,* ESIS/EGF9 (Edited by J. G. Blauel and K.-H. Schwalbe) 1991, Mechanical Engineering Publications, London, pp. 189–201.

ABSTRACT The stress and strain field ahead of crack tips in specimens and structures has been analysed numerically by means of elastic–plastic finite element analyses in order to investigate the influence of crack tip constraint and stress triaxiality on ductile crack resistance observed in fracture tests. A two-parameter approach using triaxiality-dependent local J_R curves is proposed. This gives better prediction of ductile crack growth of surface flaws.

Introduction

Crack initiation and stable crack growth in ductile materials are usually described by J resistance curves obtained from standard fracture specimens. It is known from numerous experimental investigations that the J_R curves depend on the specimen geometry and size; see, for example, **(1)(2)**. In order to prevent wrong applications, conditions for 'J control' require that crack growth should not exceed 6 percent or 1 percent of the remaining ligament for bend or tensile specimens. Nevertheless, J_R curves will be used for leak-before-break assessments as no other criteria are available.

Finite element calculations **(3)** have revealed that bend and tensile specimens differ in the triaxiality of their stress state near the crack tip. The influence of the local stress state on the tearing resistance has been widely discussed recently and different approaches have been used to quantify the local stress triaxiality and crack tip constraint **(4)–(7)**.

A common foundation for the validity of J controlled crack growth is given by the HRR theory, which postulates a J-dominated stress and strain field near the crack tip for plane problems **(8)–(10)**. In order to assure plane strain conditions and HRR-dominance, size conditions have been established for fracture specimens **(11)(12)**, see Fig. 1, but no equivalent criteria exist for structural components. Obviously the stress state near a flaw in a three-dimensional body deviates from the plane strain state. This deviation will vary along the crack front and increase with increasing plastification of the ligament. Its magnitude depends on the amount of local constraint. In a three-dimensional configuration, constraint may be applied in two directions, parallel and perpendicular to the crack front. The first or 'out-of-plane' constraint is realized by a sufficiently large thickness of the specimen and usually identified

* BAM, Unter den Eichen 87, 1000 Berlin 45, FRG.

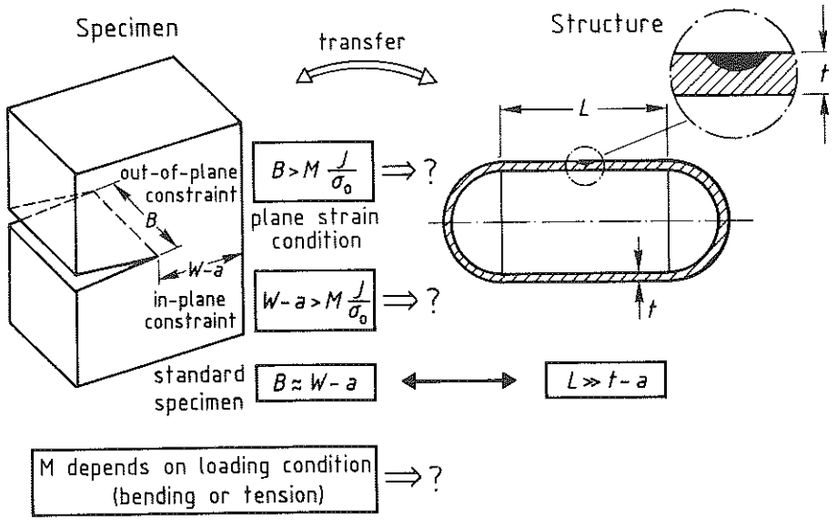

Fig 1 Constraint and size requirements

as the approach to the plane strain condition. The second or 'in-plane' constraint requires a sufficiently large ligament width of the specimen. Whereas thickness and width of specimens are usually of the same magnitude, they may differ considerably in a structure, e.g., in a pressure vessel.

This paper reports on numerical analyses of the stress and strain field ahead of crack tips in both specimens and structures with surface flaws for two different materials, viz. the German standard steels 20 MnMoNi 55 and StE 460. The approach to the HRR plane strain situation is investigated and some significant parameters describing stress triaxiality and crack tip constraint are discussed. Finally, the tearing resistance behaviour observed in fracture tests on different specimen geometries is related to the triaxiality of the stress state ahead of the crack tip. A two-parameter approach using triaxiality-dependent local J_R curves is proposed. This has given better prediction of ductile crack growth of surface flaws **(13)**.

Specimens and structures investigated

The experimental investigations **(14)(15)** cover two different steels and a number of different specimen geometries, as summarized in Table 1, and also full size pressure vessel tests with surface flaws in order to study stable crack growth in real components, Table 2. Attendant elastic–plastic finite element analyses of various specimen geometries **(14)**, Table 3, and of two vessel tests **(16)(17)** were intended not only to calculate J but also to give detailed information on the local stress and strain states in the vicinity of the cracks and thus to help to understand and explain the effect of triaxiality on the tearing

Table 1 Tearing resistance of various specimens, results from J_R curve testing

(a) *material 20 MnMoNi 5 5* (n = 7.6)

specimen	B (B_n) (mm)	W (mm)	a/W (–)	J_i (N/mm)	dJ/da (N/mm²) $\Delta a = 0.1$	1.0	2.0
CTsg	25 (19)	50	0.5	139	85	83	81
CT	25	50	0.5	115	143	149	157

(b) *material StE 460* (n = 6.0)

specimen	B (B_n) (mm)	W (mm)	a/W (–)	J_i (N/mm)	dJ/da (N/mm²) $\Delta a = 0.1$	1.0	2.0
CTsg	25 (19)	50	0.5	117	146	153	161
CT	25	50	0.5	122	244	171	91
DECT	40	500	0.8	148	147	140	132
DECT	40	125	0.8	123	183	192	203
CCTsg	20 (16)	50	0.2	141	521	296	217
CCTsg	20 (16)	50	0.5	127	544	308	225
CCTsg	20 (16)	50	0.8	130	742	277	194
CCT	40	125	0.1	94	746	506	239
CCT	40	125	0.5	149	323	265	201
CCT	40	125	0.8	100	592	541	486

resistance behaviour. As details of the experiments and calculations have been reported elsewhere **(3)(13)(15)(18)**, the following considerations will be restricted to a discussion of the experimental and numerical results with respect to the objective of the present paper. Basic information on the materials, specimen and vessel geometries is given in the tables referred to above.

Table 2 Structural and material data of the pressure vessels investigated

Test vessel				*VT1*	*VT2*
inner radius		r_i	(mm)	750	750
length of cylindrical part		L	(mm)	3000	3000
wall thickness		t	(mm)	40	398
		t/r_i	(–)	0.053	0.053
surface flaw:	*length*	$2c$	(mm)	180.4	192.1
	depth	a	(mm)	21.6	28.0
		a/c	(–)	0.239	0.292
		a/t	(–)	0.540	0.705
material				20 *MnMoNi* 55	*StE* 460
yield strength		R_{eL}	(MPa)	460	490
ultimate stress		R_m	(MPa)	604	642
Ramberg–Osgood		n	(–)	7.1	7.4
		α	(–)	2.3	2.6
pressure:	*ligament yielding*	p_y	(MPa)	17.5	21.0
	crack growth initiation	p_i	(MPa)	22.4	20.0
	end of test	p_{max}	(MPa)	24.2	22.4

Table 3 Comparison of global and local parameters characterizing fracture behaviour of specimens, results from finite element calculations

(a) material 20 MnMoNi 5 5(n = 7.6), FE analysis of non-growing crack

specimen	W (mm)	a/W (–)	FE-model	L (–)	d_n^{-1} (–)	$K_{\sigma p}$* (–)	χ* (–)
CT	50	0.5	*pl. strain*	1.69	2.35	4.1	2.9
DECT	125	0.8	*pl. strain*	1.70	2.01	3.8	2.5
CCT	125	0.8	*pl. strain*	1.18	1.68	3.3	1.7
CCT	125	0.1	*pl. strain*	1.16	1.70	3.4	1.8
CCT	125	0.1	*pl. stress*	1.02	1.30	—	0.5
CT	25	0.5	*3D, z = 0*	1.47	2.47	4.0	2.2
CT	50	0.5	*3D, z = 0*	1.46	2.26	4.2	2.5
CT	200	0.5	*3D, z = 0*	1.47	2.31	4.2	2.9
CT	400	0.5	*3D, z = 0*	1.47	2.32	4.1	2.9

* *for* J ≃ *150 N/mm*, Δa = *0*

(b) material StE 460 (n = *6.0*), *numerical simulation of crack growth*

specimen	W (mm)	a/W (–)	FE-model	L (–)	d_n^{-1} (–)	$K_{\sigma p}$† (–)	χ† (–)
CT	50	0.6	*pl. strain*	1.58	1.88	3.6	2.8
CCT	50	0.5	*pl. strain*	1.16	1.30	3.3	1.5

† *for* J ≃ *105 N/mm*, Δa = *0*

HRR-dominance

The asymptotic solution for stresses and strains at the tip of a non-growing crack in a power law hardening material, which is known as 'HRR', shows J as an intensity parameter of the singular field quantities. Thus, in addition to energy balance considerations based on Griffith's concept, there is a second foundation for using J as a characteristic fracture parameter based on Irwin's stress intensity concept. As long as the 'real' stresses and strains at the crack tip in a flawed structure are dominated by J, the latter will be an appropriate quantity for defect assessment. Consequently much attention has been paid to investigating under which conditions and to what extent the real stresses approach the HRR plane strain solution **(8)–(10)** which can be supposed to be the most severe stress state. Examples from two- and three-dimensional numerical analyses of a compact specimen and a pressure vessel with surface crack are shown in Figs 2 and 3, where the maximum principle stresses, σ_{yy}, in the crack ligament as obtained from finite element (FE) calculations are related to the respective values of the HRR plane strain solution. The distance to the crack tip, r, on the abscissa has been made dimensionless by the crack tip opening displacement (CTOD), δ_t, using the well known relationship

$$\delta_t = d_n \frac{J}{R_{eL}}. \tag{1}$$

As the HRR field is an asymptotic solution, the 'FE stresses' will approach the 'HRR stresses' in a small region close to the crack tip only. In addition, the

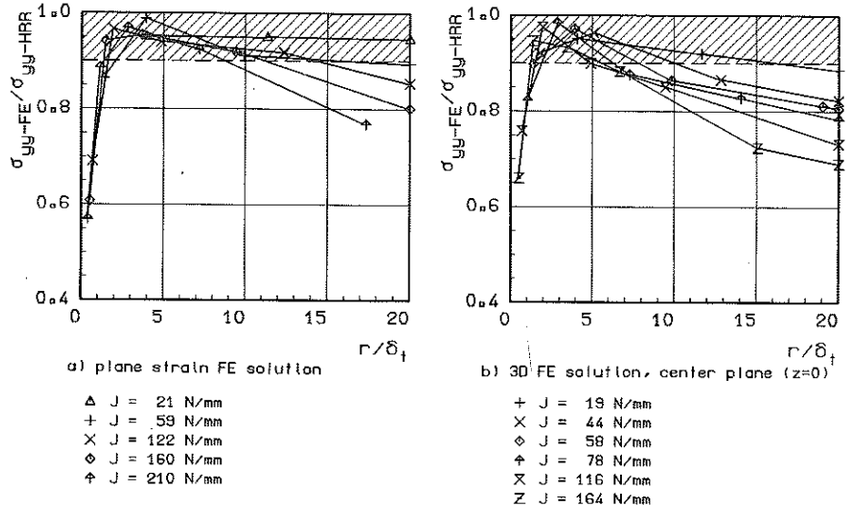

Fig 2 HRR-dominance near the crack front of a compact specimen CT-25 (20 MnMoNi 55), first principle stress from FE calculation related to HRR solution for increasing load

plastic crack tip blunting does not allow the stresses to become singular for $r \to 0$ if the analysis accounts for large deformations **(19)**. A measure for HRR-dominance may be defined by postulating that $0.9 \leqslant \sigma_{yy,\,FE}/\sigma_{yy,\,HRR} \leqslant 1.0$ is reached over some finite distance **(10)**. Whereas there is apparently HRR-

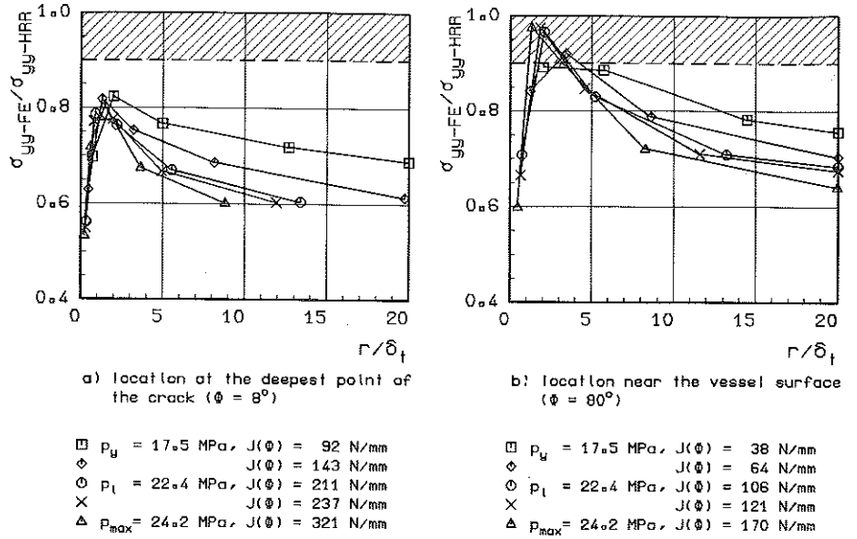

Fig 3 HRR-dominance near the crack front of a pressure vessel with semi-elliptical surface flaw (VT1, 20 MnMoNi 55), first principle stress from FE calculation related to HRR solution for increasing pressure (see Table 2)

dominance for the plane strain model and in the midplane of a 3D model of a compact specimen, Figs 2(a) (b), the situation is different at the crack front of the surface flaw in the pressure vessel, Figs 3(a) (b). Close to the centre line of the semi-elliptical flaw, which is the point of maximum crack depth and denoted by the parametric angle $\Phi = 0$ degrees, the stresses reach only about 80 percent of the HRR values, Fig. 3(a). HRR-dominance is much better realized in the region of axial extension of the crack, e.g., $\Phi = 80$ degrees as shown in Fig. 3(b), where $\Phi = 90$ degrees denotes the intersection of the crack front with the vessel surface. Hence, it is not to be expected that the same J_R curve will be valid for ductile crack growth in wall thickness and in axial direction. This is obviously due to the differing 'in-plane constraint', as the wall thickness is small compared with the vessel length, resulting in a differing 'triaxiality' of the stress state. The problem still to be solved is how to define and quantify 'constraint' and 'triaxiality' in a significant, reliable, and reproducible manner.

Crack tip constraint and triaxiality of stresses

A common global measure of constraint is the plastic constraint factor, L, defined by the ratio of the actual general yield load of a flawed structure and its plastic limit load referring to the net section. This factor makes it possible to set up a rank correlation between different specimen geometries, see Table 3, but it is not suited to characterize the local variation of crack tip constraint in a structure.

Instead of this, the relationship between the CTOD, δ_t, and J, derived from HRR theory and given in equation (1), may be used as a significant local quantity (4) as less CTOD means more crack tip constraint. The ratio d_n^{-1} depends on the hardening exponent, n, see Fig. 4(a). For comparison the results of FE calculations for various specimen geometries are also given in this figure. Unfortunately the dependency on n outweighs the difference between plane strain and plane stress for $n \leqslant 5$. The variation of d_n^{-1} along the crack front of the two semi-elliptical surface flaws is plotted in Figs 5(a) (b), indicating that the highest crack tip constraint is reached near $\Phi = 80$ degrees. From an overall point of view, the range of values is not very wide, thus restricting the quantitative significance of this ratio, although its numerical reliability is satisfying.

The tensile stress criterion relies on the maximum principle stress. Thus for cleavage fracture phenomena the plastic stress concentration factor

$$K_{\sigma p} = \max_r \left(\frac{\sigma_{yy}(r, \theta)}{R_{eL}} \right)_{\theta=0} \qquad (2)$$

is relevant. It establishes the same hierarchy of specimen geometries as L and d_n^{-1}, see Table 3, and it also shows a weak maximum near $\Phi = 80$ degrees for the surface flaws, see Figs 5(a)(b). However, as normal stresses in FE calcu-

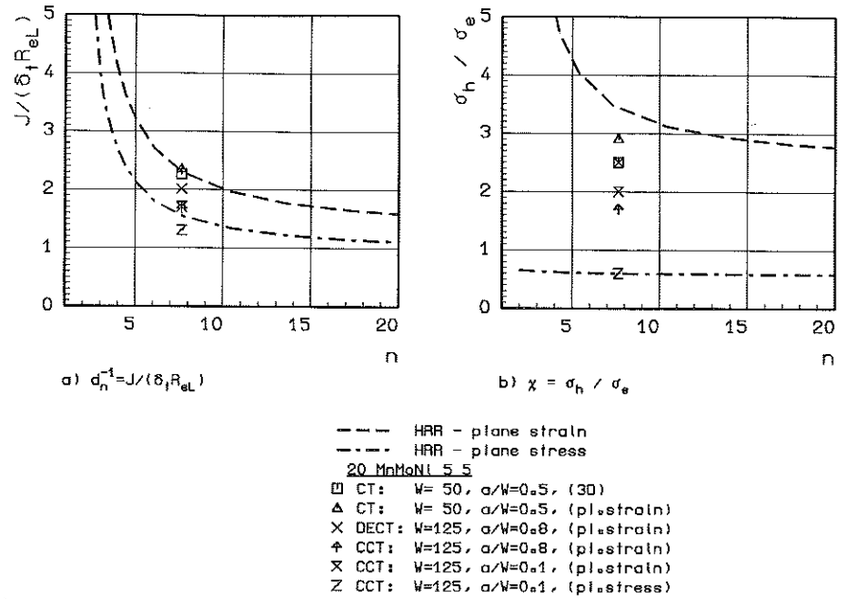

Fig 4 Crack tip constraint and triaxiality factors from HRR theory dependent on hardening exponent n

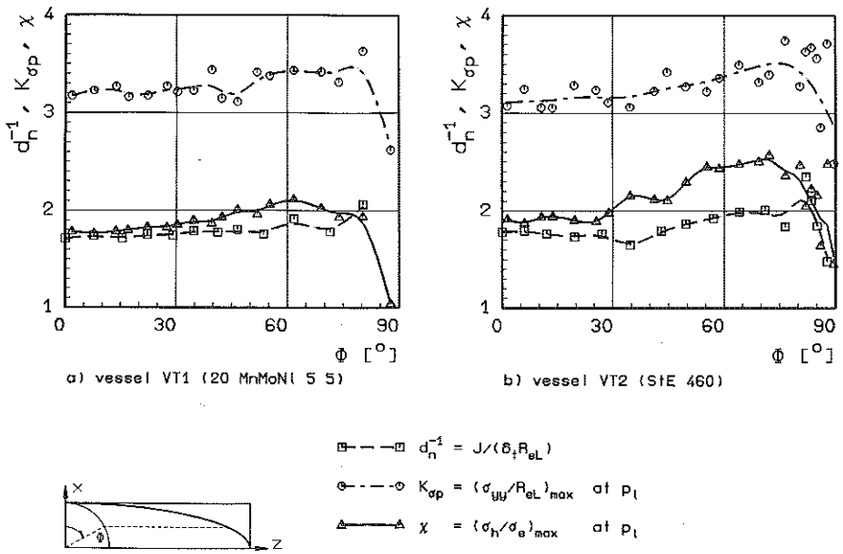

Fig 5 Pressure vessel with semi-elliptical surface flaw, local crack tip constraint, stress concentration, and triaxiality

lations are subject to numerical oscillations near the crack front, its reliability is limited.

Attempts to define stress triaxiality in plastic fracture date back to Hencky's diagram **(20)** of effective shear stress, τ_r, versus hydrostatic stress, σ_h, from which Clausmeyer **(21)** derived the ratio

$$q = \frac{\tau_r}{\sigma_h} = \frac{\sigma_e}{\sqrt{(3)}\sigma_h} = \frac{\sqrt{(\sigma'_{ij}\,\sigma'_{ij})}}{\sqrt{(2)}\sigma_{ii}} \tag{3}$$

This ratio varies not only with the crack front coordinate but with the distance to the crack front and the ligament angle. Hence, an additional assumption has to be made in order to decide which value is to be taken. This may be its maximum ahead of the crack tip or the value at some critical length. Besides, it is not quite satisfying to use a ratio of triaxiality giving a *de*creasing number with *in*creasing triaxiality just because Hencky has plotted σ_h on the abscissa, and τ_r on the ordinate.

Ductile crack growth is characterized by micro-mechanical processes of void nucleation, growth, and coalescence. McClintock **(22)** and Rice and Tracey **(23)** found that the growth rate of cavities in perfectly plastic materials is proportional to $\exp(3\sigma^\infty/2\sigma_0)$, where σ^∞ and σ_0 are the remote mean or hydrostatic stress and the yield stress respectively. For a hardening material the yield stress equals the actual von Mises effective stress, σ_e, under fully plastic conditions. Apart from the multiplying coefficient, the exponential is equal to q^{-1}. We will therefore define

$$\chi = \max_r \left(\frac{\sigma_h(r,\,\theta)}{\sigma_e(r,\,\theta)} \right)_{\theta=0} \tag{4}$$

as the local triaxiality for any point of the crack front, continuing previous considerations **(3)(13)**. In HRR theory, χ is constant with respect to r and depends on the hardening exponent n as plotted in Fig. 4(b), showing that the range of values between the limiting cases of plane strain and plane stress is much wider than for d_n^{-1}, giving χ a much better quantitative significance. Again, the results of FE calculations of various specimen geometries are shown for comparison. The variation of $\chi(\Phi)$ along the crack front of the surface flaws is shown in Figs 5(a)(b). The curves had to be smoothed by spline functions because of numerical oscillations. They show the same tendency as those of $K_{\sigma p}(\Phi)$ and $d_n^{-1}(\Phi)$.

It still cannot be decided which of the three parameters defined by equations (1), (2) and (4) is to be preferred.

Tearing resistance and triaxiality

Whereas the critical J value for crack growth initiation, J_i, is supposed to be a material constant and thus not to depend on geometry effects, the J_R curves of different specimen geometries differ with increasing crack growth, Δa. Their

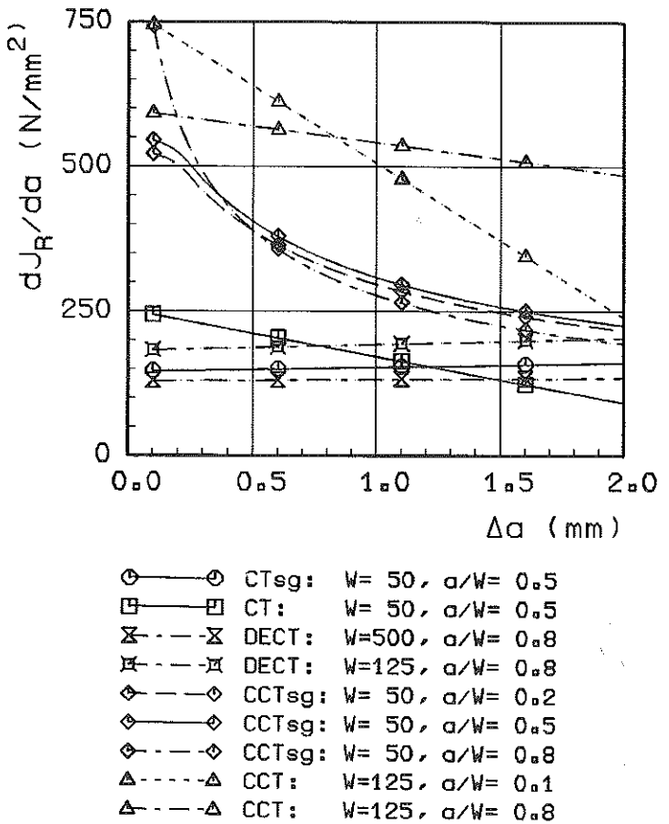

Fig 6 Tearing resistance dJ/da for various specimens (StE 460)

slope, dJ/da, is called tearing resistance. It is plotted in Fig. 6 for a number of different specimen geometries of the steel StE 460 **(15)**. Some general tendencies can be observed. The tearing resistances of compact and large double edge cracked specimens do not differ significantly and, with the exception of the non-side-grooved CT specimen, remain constant with increasing Δa. The centre cracked panels start with high values of tearing resistance which, with increasing Δa, decrease more or less to those of the CT and DECT specimens, depending whether or not the CCT specimens are side-grooved. A crack growth analysis should account for all of these phenomena.

As the progress of the local crack advance could not be measured in the vessel tests **(14)**, only average values, $\Delta J/\Delta a$, of the local tearing resistance could be calculated for the surface flaws, see Fig. 7, which conceal any dependence on Δa. Nevertheless, the curves admit the interpretation that high constraint, Fig. 5, is correlated with low tearing resistance and vice versa. The dashed horizontal lines indicate the tearing resistance of side-grooved compact

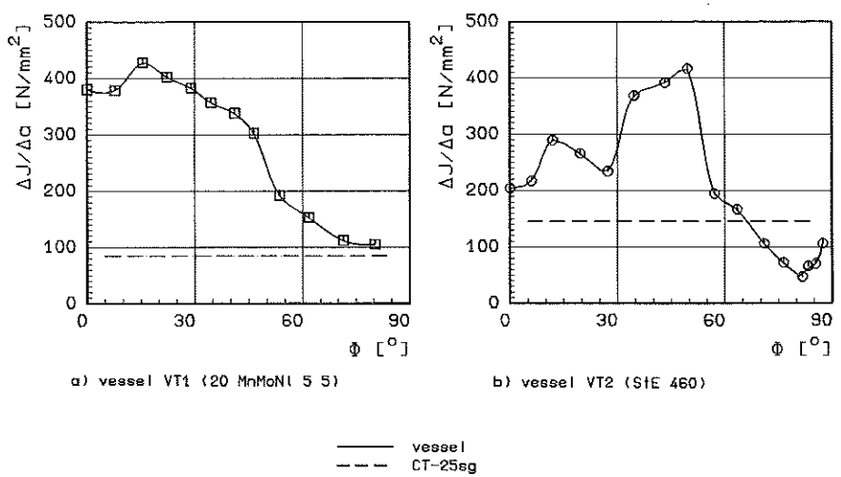

Fig 7 Local tearing resistance $\Delta J/\Delta a$ for a semi-elliptical surface flaw in a pressure vessel

specimens of the respective materials. It has also been shown previously **(3)** that the triaxiality defined by equation (4) can be correlated with the slopes of J_R curves obtained for different specimen geometries. The idea of relating dJ/da and χ **(5)(6)(13)(18)** is therefore obvious, and all that is needed is an appropriate function.

Assuming that upper and lower limits exist for the tearing resistance which correspond to the limiting cases of plane strain and plane stress respectively an approximation function was found **(13)(18)** by

$$\frac{dJ}{da}(\chi) = A + B \tanh \frac{D - \chi}{C} \tag{5}$$

The constants in equation (5) are given by

$$A = \frac{1}{2}\left[\left(\frac{dJ}{da}\right)_{\text{pl. stress}} + \left(\frac{dJ}{da}\right)_{\text{pl. strain}}\right]$$

$$B = \frac{1}{2}\left[\left(\frac{dJ}{da}\right)_{\text{pl. stress}} - \left(\frac{dJ}{da}\right)_{\text{pl. strain}}\right]$$

$$C = -B\left[\frac{d}{d\chi}\left(\frac{dJ}{da}\right)\right]^{-1}_{\chi = D}$$

$$D = \tfrac{1}{2}[\chi_{\text{pl. stress}} + \chi_{\text{pl. strain}}] \tag{6}$$

The χ values for plane strain and plane stress can be calculated from the HRR solutions, see Fig. 4, and the corresponding (dJ/da) values are obtained approximately from R curves of side-grooved compact specimens and centre cracked panels respectively.

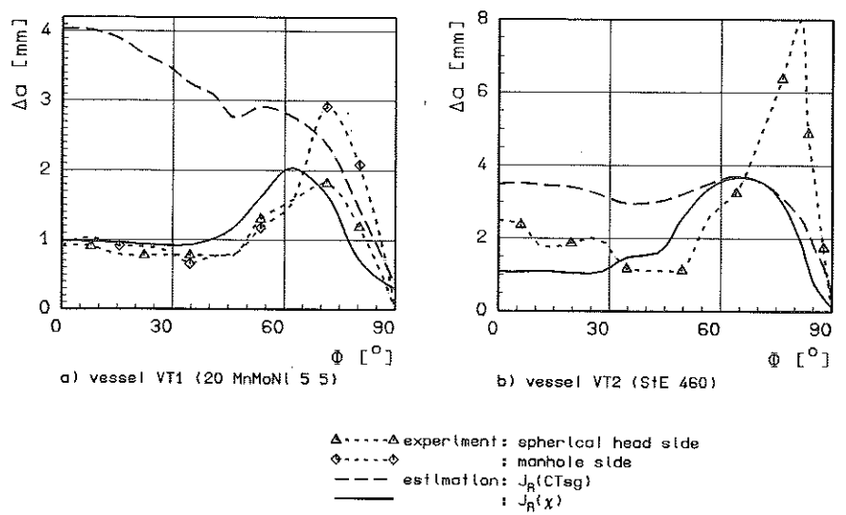

Fig 8 Local ductile crack growth for a semi-elliptical surface flaw in a pressure vessel, experiment, and estimation

The resulting predictions of $\Delta a(\Phi)$ for the two vessel tests based on both the J_R curve of a compact specimen and local χ-dependent tearing resistance are plotted in Fig. 8. The concept of a unique characteristic $J(\Delta a)$ overestimates the real crack growth for VT1 at $\Phi = 0$ degrees in wall thickness direction up to four times and is not able to predict the maximum crack growth for VT1 and VT2 at $\Phi = 70$ degrees and 80 degrees respectively. Thus it may yield non-conservative estimates with respect to a leak-before-break assessment. The improved concept of local J_R curves depending on the triaxiality of stresses gives a much better qualitative and quantitative explanation of the ductile crack growth for VT1. It also gives a qualitatively better prediction of $\Delta a(\Phi)$ for VT2, i.e., it reflects the ratio Δa_{max}: Δa_{min} obtained in the experiment as well as the approximate position of Δa_{max}. The quantitative results for VT2 are still poor, however, which might be due to the restriction that the analysis, despite the rather large crack growth, did not account for changes in the crack shape geometry in the calculation of J and χ.

Conclusions

The geometry effect on J_R curves can be quantified by introducing an appropriate measure of either the crack tip constraint or of the triaxiality of the stress state. The former may be defined as the ratio of J and CTOD, the latter as the ratio of hydrostatic and effective stress. Both quantities seem to be equivalent as they give the same rank correlation for specimen geometries and showed a similar variation along the crack front of surface flaws.

A satisfactory agreement between structural and specimen crack growth behaviour will only be obtained if the effect of locally varying crack tip constraint or stress triaxiality is taken into account by introducing dJ/da curves which depend on either of the two quantities. This might also overcome the limit conditions for 'J-controlled' crack growth.

The present FE analysis did not simulate crack growth and thus did not account for any changes of the J or χ variation along the crack front due to the changing crack configuration. The dJ/da curves of CT and CCT-specimens suggest that triaxiality will remain constant during crack growth in bend specimens but increase in tensile specimens.

Acknowledgements

The results reported here were obtained in the course of research supported by the Bundesminister für Forschung und Technologie of the Federal Republic of Germany.

References

(1) GARWOOD, S. J. (1979) Effect of specimen geometry on crack growth resistance, *ASTM STP 677*, pp. 511–532, ASTM, Philadelphia.
(2) SCHWALBE, K.-H. and HELLMANN, D. (1984) Correlation of stable crack growth with the J-integral and the crack tip opening displacement, effects of geometry, size and material, *Report GKSS 84/E/37*, GKSS-Forschungszentrum Geesthacht (FRG).
(3) BROCKS, W., KÜNECKE, G., NOACK, H.-D., and VEITH, H. (1989) On the transferability of fracture mechanics parameters to structures using FEM, *Nucl. Engng Des.*, **112**, 1–14.
(4) STEENKAMP, P. A. J. M. (1986) Investigation into the validity of J-based methods for the prediction of ductile tearing and fracture, *PhD thesis*, Technical University of Delft.
(5) KORDISCH, H., SOMMER, E., and SCHMITT, W. (1987) Einfluß der Mehrachsigkeit auf das stabile Rißwachstum, Berichtsband 13, MPA-Seminar, Band 1, Stuttgart, Materialprüfanstalt, 7.1–7.17.
(6) AURICH, A. and SOMMER, E. (1988) The effect of constraint on elastic–plastic fracture, *Steel research*, **59**, 358–367.
(7) CLAUSMEYER, H., KUßMAUL, K., and ROOS, E. (1989) Der Einfluß des Spannungszustandes auf den Versagensablauf angerissener Bauteile aus Stahl, *Mat.-wiss. und Werkstofftechn.*, **20**, 101–117.
(8) McMEEKING, R. M. and PARKS, D. M. (1979) On criteria for J-dominance of crack-tip fields in large scale yielding, *ASTM STP 668*, pp. 175–194, ASTM, Philadelphia.
(9) SHIH, C. F. and GERMAN, M. (1985) Requirements for a one parameter characterization of crack tip fields by the HRR-singularity, *Int. J. of Fracture*, **29**, 73–84.
(10) SHIH, C. F. (1985) J-dominance under plane strain fully plastic conditions: the edge crack panel subject to combined tension and bending, *Report DOE/ER/10556/102*, Providence, Brown University.
(11) AMERICAN SOCIETY FOR TESTING AND MATERIALS (1981) Standard test method for J_{Ic}, a measure of fracture toughness, *ASTM E 813*, ASTM, Philadelphia.
(12) DEUTSCHER VERBAND FÜR MATERIALPRÜFUNG (1987) Ermittlung von Rißinitiierungswerten und Rißwiderstandskurven bei Anwendung des J-Integrals, *DVM-Merkblatt*, **002**, Berlin.
(13) BROCKS, W. and KÜNECKE, G. (1989) Elastic–plastic fracture mechanics analysis of a pressure vessel with an axial outer surface flaw, *Nucl. Engng and Des.*, **112**, 1–14.
(14) AURICH, D. *et al.* (1987) Analyse und Weiterentwicklung bruchmechanischer Versagenskonzepte auf der Grundlage von Forschungsergebnissen auf dem Gebiet der Komponentensicherheit, Teilvorhaben, *Werkstoffmechanik, Forschungsbericht*, **137**, Bundesanstalt für Materialforschung und- prüfung, Berlin.
(15) AURICH, D., WOBST, K., and KRAFKA, H. (1989) J_R curves of wide plates and CT25 specimens – comparison of the results of a pressure vessel, *Nucl. Engng Des.*, **112**, 319–328.
(16) BROCKS, W., KÜNECKE, G., and MÜLLER, W. (1988) Elastic–plastic fracture mechanics analysis of a pressure vessel with an axial outer surface flaw (part 1), Technical Report for RS 1500 490, *Analysis and further development of fractures mechanics failure concepts based on research data in the field of integrity of components*, Berlin: Bundesanstalt für Materialforschung und- prüfung.
(17) BROCKS, W. and KÜNECKE, G. (1989) Elastic–plastic fracture mechanics analysis of a pressure vessel with an axial outer surface flaw (part 2), Technical Report for RS 1500 490, *Analysis and further development of fractures mechanics failure concepts based on research data in the field of integrity of components*, Berlin: Bundesanstalt für Materialforschung und- prüfung.
(18) BROCKS, W., KÜNECKE, G., and WOBST, K. (1989) Stable crack growth of axial surface flaws in pressure vessels, *Int. J. Pres. Ves. & Piping*, **39**, 77–90.
(19) BROCKS, W. and OLSCHEWSKI, J. (1986) On J-dominance of crack-tip fields in largely yielded 3D structures, *Int. J. Solids Structures*, **22**, 693–708.
(20) HENCKY, H. (1943) Ermüdung, Bruch, Plastizität, *Stahlbau*, **16**, 95–97.
(21) CLAUSMEYER, H. (1968) Über die Beanspruchung von Stahl bei mehrachsigen Spannungszuständen, *Konstruktion*, **20**, 395–401.
(22) McCLINTOCK, F. A. (1968) A criterion for ductile fracture by the growth of holes, Trans. ASME, *J. Appl. Mech.*, **35**, 363–371.
(23) RICE, J. R. and TRACEY, D. M. (1969) On the ductile enlargement of voids in triaxial stress fields, *J. Mech. Phys. Solids*, **17**, 201–217.